analytical chemistry

pubs.acs.org/ac Article

Temperature-Alternated Electrochemical Aptamer-Based Biosensor for Calibration-Free and Sensitive Molecular Measurements in an Unprocessed Actual Sample

Zhi-min Chen, Yi Wang, Xing-yuan Du, Jian-Jun Sun,* and Sen Yang*

Cite This: *Anal. Chem.* 2021, 93, 7843−7850 Read Online

ACCESS | Metrics & More | Article Recommendations | Supporting Information

ABSTRACT: Frequently calibrating electrochemical biosensors (ECBs) to obtain acceptable accuracy can be cumbersome for the users. Thus, the achievement of calibration-free operation would effectively lead to commercial applications for ECBs in the real world. Herein, we fabricated a temperature-alternated electrochemical aptamer-based (TAEAB) sensor, producing a cycle of "enhanced-responsive and ∼nonresponsive" state at rapidly alternated interface temperatures (5 and 30 °C, respectively). The ratio of peak currents collected at two temperatures overcomes sensor-to-sensor fabrication variations, obviating sensor calibration prior to use due to its good reproducibility. We then demonstrated the capability of TAEAB sensors for improved, sensitive, and calibration-free measurement of different targets within 7 min, which respectively achieved a detection limit of 0.5 μM procaine in undiluted urine and 1.0 μM adenosine triphosphate in undiluted serum. This generalizable approach ameliorates sensitivity without the complicated amplification step, thus simplifying the operation procedure and reducing the detection time, which will effectively improve the clinical utility of biosensors.

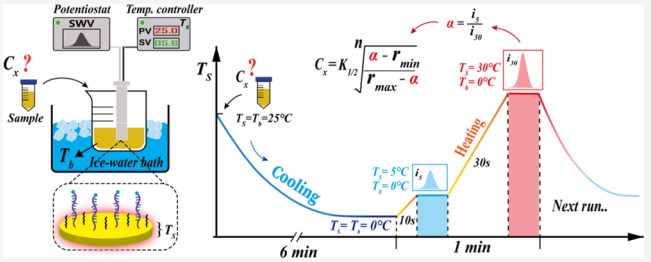

To preserve the accuracy of the commercial continuous glucose monitor (<20% error[1]), the instruction of manufacturers recommends a calibration at least every 12 h.[2] Although this method has a clear clinical value,[3] it will reduce convenience and introduce opportunities for user errors.[4,5] The need to perform calibration operation will discourage many potential users, and it has proven to be one of several hurdles impeding electrochemical biosensor (ECB)[6] applications in clinical diagnostics or field-portable devices.[7,8] Thus, the development of calibration-free sensing approaches will greatly improve the usability of ECBs and enhance market adaptation and acceptance. Of note, our concept of "calibration-free" here refers to the fact that the sensor can be pre-calibrated in the factory and used as is, allowing for a "determined-once-for-all" model.[9,10]

A substantial amount of work has been devoted to pushing the detection limits and sensitivities of biosensors, but little attention has been paid to sensor calibration and validation in real samples.[11,12] Only a few calibration-free biosensing approaches[9,10,13] have been developed to increase the adaptation and clinical utility of ECBs. For example, Tarasov and co-workers realized an on-site calibration-free biosensor by using "differential" readout of pairs of differently functionalized, antibody-modified electrolyte-gated field-effect transistors.[14] However, the signal transduction mechanism of this sensor depends on the specific chemical reactivity of their target; thus, this strategy is not generalizable to the measurement of other molecules.

Electrochemical aptamer-based (E-AB) sensors[15] are a widely used sensing platform for reagentless, rapid, and specific analyte detection in complex matrices[16−19] and even the living animals.[20] E-AB sensors employ a redox-reporter-modified, structure-switching aptamer as their recognition element, and a target binding-induced conformational change alters the electron transfer (ET) between the reporter and interrogated electrode surface.[21] Due to this reversible signal transduction mechanism,[22,23] the sensor is cost-effective and supports real-time measurement, which is suitable for the development of point-of-care testing (POCT)[24] or continuous sensing applications.[17] However, traditional E-AB sensors need to circumvent sensor-to-sensor signal variations by calibrating each individual sensor by a zero-target standard solution prior to use.[4] Such calibration is inconvenient, and more importantly, it is hard to perform this operation when sensors are deployed directly in actual samples with target molecules such as undiluted serum, urine, and even whole blood.

Received: January 21, 2021
Accepted: May 11, 2021
Published: May 24, 2021

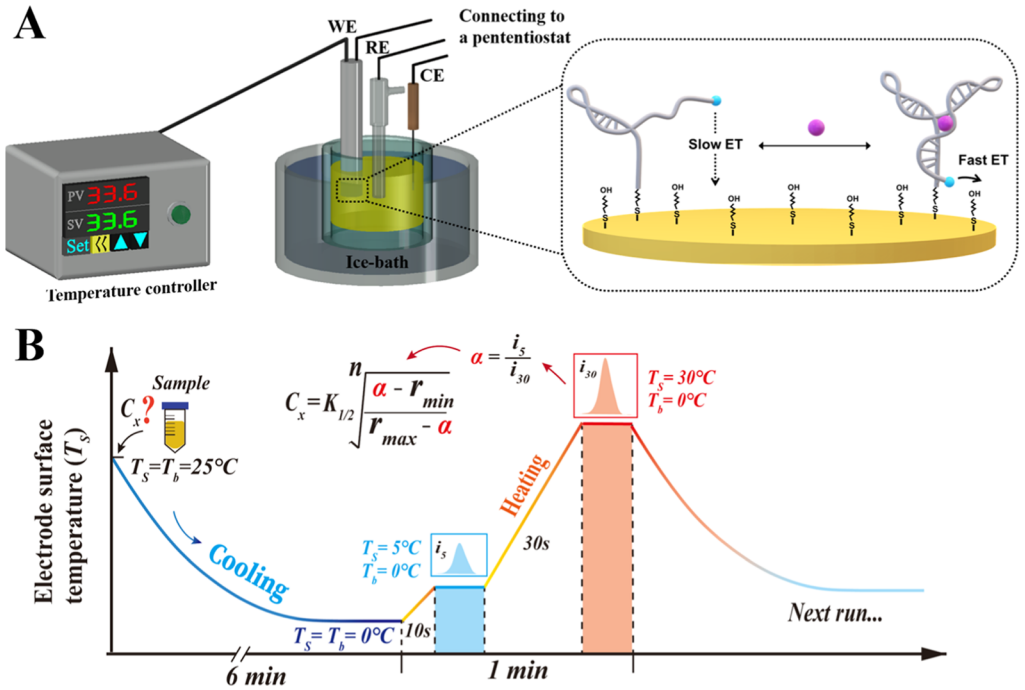

Figure 1. Schematic diagram of TAEAB sensors and the detection process. (A) TAEAB sensors consist of an electroactive reporter-modified, thiolated aptamer (here, a three-way-junction-structured aptamer is shown) and a temperature-controllable gold disk electrode (Au-TCDE). The binding of the aptamer and target molecules (purple ball) will induce a conformational change, which alters the ET kinetics between the reporter [blue ball: methylene blue (MB)] and the electrode. This produces a target concentration-dependent change in current when the sensor is interrogated *via* the square wave voltammetry.[4] We modified a Au-TCDE with structure-switching aptamers, whose surface temperature (T_s) can be rapidly alternated in an ice-water bath (0 °C). (B) Sensitive, rapid, and accurate analyte concentration determination *via* TAEAB sensors. T_b and T_s represent the temperature of bulk sample solution and electrode surface, respectively. The samples and the sensors are immersed in an ice-water bath for a few minutes until T_b = T_s = 0 °C (3 mL solution cooling for ∼6 min). We first use one set of sensors to determine the calibrated parameters ($K_{1/2}$, n, r_{min}, and r_{max} from Hill equation, eq 1) for this class of sensor, and these parameters remain the same from sensor to sensor, allowing for a "determined-once-for-all" model. Thus, without the need for calibration operation, sample pretreatment process, and redundant operation steps, we only need to measure the ratio (α) of two peak currents at 5 and 30 °C for estimating the target concentration accurately.

Therefore, Plaxco and co-workers reported calibration-free operating E-AB biosensors using two different ratiometric strategies. First of all, the E-AB signal is a strong function of square-wave frequency (when using square-wave voltammetry to monitor target-dependent current change), producing "signal-off," "signal-on," or "nonresponsive" behaviors.[25] The ratio of two currents at responsive and nonresponsive frequencies is largely insensitive to drift and sensor-to-sensor fabrication variations; thus calibration-free operation of sensors can be achieved.[4,26,27] Another one is the "dual reporter" approach,[5] achieving calibration-free measurements of adenosine triphosphate (ATP) or kanamycin *in vivo*. A "reference" reporter served as an internal reference that does not respond to the presence of the target, allowing us to correct for sensor-to-sensor variability. Recently, Li *et al.* employed one probe-attached redox reporter and a second intercalated redox reporter to generate two signals, obviating the need for calibration as their ratio remains reproducible.[28] These strategies obviate the need for calibrating each individual sensor without damaging sensitivity or selectivity.

Here, we fabricated a "temperature-alternated electrochemical aptamer-based (TAEAB) sensor" (Figure 1A) for improved, sensitive, calibration-free molecular measurements in unprocessed actual samples. We modified temperature-controllable gold disk electrodes (Au-TCDEs)[29] with structure-switching aptamers. The Au-TCDE immersed in ice-water bath can rapidly change electrode surface temperature (T_s), which will generate temperature-difference (ΔT_{bs}) between T_s and the bulk solution (T_b).[30,31] We then demonstrated that the E-AB signal is also a strong function of interface temperature, producing "enhanced-responsive" and "∼nonresponsive" signal outputs at the given T_s (5 and 30 °C). The ratio of two peak currents collected at different T_s overcomes sensor-to-sensor fabrication variations and sensor degradation. Then, the Hill equation is used to determine the "factory" parameters that remain the same for this class sensor. Thus, it obviates the calibration of each individual sensor prior to their use. TAEAB sensors could rapidly and easily determine target concentration *via* the ratio output without the calibrated operation and sample pretreatment and greatly shorten the turnaround time of sample to sample (Figure 1B). Due to the easy-to-deploy cooling device (ice-water bath is a readily available setup) and user-friendly two-step detection operation, our strategy significantly promotes the practical utility of biosensors. Therefore, TAEAB sensors are promising for enabling more widespread small-molecule analysis in clinical practice, which lays a foundation for future real-world applications.

EXPERIMENTAL SECTION

Materials. Procaine hydrochloride, tris(2-carboxyethyl) phosphine, and 6-mercapto-1-hexanol were purchased from Aladdin Co., Ltd. (Shanghai, China). Trizma preset crystals, at pH 7.4, were purchased from Sigma-Aldrich, St. Louis, MO, USA. Fetal calf serum was purchased from Tianhang Biotechnology Co., Ltd (Zhejiang, China). Fresh urine was

https://doi.org/10.1021/acs.analchem.1c00289
Anal. Chem. 2021, 93, 7843−7850

taken from a healthy human and filtered (0.22 μM) before use. Of note, 1 ml of 1 ppm cocaine was obtained from Xiamen Pushi nanotechnology Co., Ltd (Fujian, China). All reagents were used as received. Thiol-modified DNA aptamer sequences were synthesized by Sangon Biotechnology Co., Ltd. (Shanghai, China), purified by high-performance liquid chromatography (HPLC), and confirmed by the HPLC profile and mass spectrometry. These were dissolved in 10 mM Tris-HCl buffer to a final concentration of 100 μM, aliquoted, and stored at −20 °C prior to use. Aptamer sequences used in this work are listed below as previously reported[32,33] (SH-C6 = 6-carbon thiol linker, MB = methylene blue):

Procaine and cocaine aptamer: 5′-SH-C6-AGA CAA GGA AAA TCC TTC AAT GAA GTG GGT CT-MB-3′

ATP aptamer: 5′-SH-C6-CTT ACG ACT GAG AAG TGT GAT TCA GTA TGT TTT C-MB-3′

All aqueous solutions were prepared using 18.25 MΩ cm^{-1} ultrapure water (Research Scientific Instruments Co., Ltd., Shanghai, China).

Temperature-Dependent Electrochemical Measurements. Square wave voltammetry (SWV) was performed using a potential window of 0.0 to −0.5 V, using an amplitude of 25 mV and a potential step of 1 mV for 200 Hz. T_s and T_b represent the electrode surface temperature and the bulk solution temperature in this article, respectively.

In the overall temperature-changing ($T_{overall}$) approach (Figure 2A), the overall detecting system (sample solution and three-electrode setup), where T_b is equal to T_s, can be cooled to 5, 10, 15, 20, and 25 °C using a cryogenic incubator (Xinxing Instruments Co., Ltd, Cangzhou, Hebei, China). In addition, a thermostat water bath (DK-8D, Boxun Co., Ltd, Shanghai, China) is used to heat the sample solution to 25 (if room temperature is lower than 25 °C), 30, and 35 °C. The solution temperature is monitored by a thermometer.

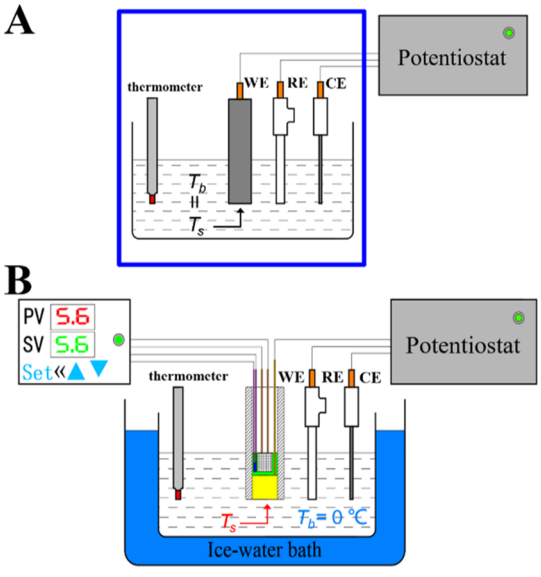

Figure 2. Device diagram of two different temperature-changing approaches. WE: working electrode (temperature-controllable disk electrode, TCDE), RE: saturated Ag/AgCl electrode, CE: platinum wire. (A) Overall temperature-changing ($T_{overall}$) approach. Blue line represents a cryogenic incubator. (B) Heated electrode temperature-changing (T_{heated}) approach.

In the heated electrode temperature-changing (T_{heated}) approach (Figure 2B), the cell was placed in an ice-water bath, in which $T_b = 0 \pm 0.3$ °C (measured by a thermometer). T_s can be heated from 0 to 5, 10, 15, 20, 25, 30, and 35 °C by a temperature controller. The display temperature of the thermostat control panel (PV) is the temperature of the heating module inner electrode. T_s can be obtained by the temperature transfer coefficient and the structural model conversion, as mentioned in the literature.[29] For example, T_s is 5/30 °C, corresponding to heating temperature 5.6/33.6 °C when T_b = 0 °C. The heating electrode surface hardly affects T_b. For example, T_b will increase to 1.6 ± 0.6 °C when T_s = 30 °C. For the convenience of description, T_b is taken as 0 °C in this article. The signal gain at 0 °C is tested through emplacing the sensor and the cell in an ice-water bath. We then converted the raw current of each sensor into signal gain (%) using the following equation

$$\text{signal gain} = (I_{target} - I_{blank})/I_{blank} * 100\%$$

RESULTS AND DISCUSSION

Temperature-Dependent E-AB Response. Aptamer–target interactions are significantly influenced by environmental conditions; in particular, the binding affinity between aptamers and target molecules is strongly related to temperature. However, we still lack a systematic understanding of the signal response of E-AB sensors directly affected by temperature. To illustrate this, we employed two temperature-changing approaches to explore the effect of temperature on E-AB sensors (Figure 2). The aptamer-modified Au-TCDEs immersed in an ice-water bath can rapidly change the electrode surface temperature (T_{heated} approach). The overall temperature change ($T_{overall}$) approach is used as a control group (Figure 2A). We observed a large variation in the signal gain of procaine sensors for each testing temperature controlled by $T_{overall}$ or T_{heated} approach (Figures S1 and S2). The signal gain greatly increases at low temperatures (<25 °C) and decreases at elevated temperatures (>25 °C). We believe that this is as a result of the temperature-dependent binding affinity.[34−36] Interestingly, comparing with the $T_{overall}$ approach (with same T_s), the T_{heated} approach produces a larger signal output at 5 °C and gets a worse signal at 30 °C (Figure S1: red and gray shade). This result is possibly related to the thermal convection caused by temperature difference (ΔT_{bs}) between the electrode surface and the bulk sample solution.[31]

To further illustrate it, the calibration curve is performed in different temperature conditions (Figures S3 and S4). We then fit the obtained target dose response profiles with the Hill equation (eq 1)[28] to determine the related dissociation constant $K_{1/2}$ (Table 1). The Hill equation is as follows

$$\text{signal gain} = r_{min} + (r_{max} - r_{min})\frac{[\text{target}]^n}{({K_{1/2}}^n + [\text{target}]^n)} \quad (1)$$

where n is the Hill coefficient, r_{min} and r_{max} are the minimum and maximum values of the response signal (*i.e.*, when the sensors are challenged in the absence or presence of a saturating target, respectively), and dissociation constant $K_{1/2}$ is the midpoint of the target dose–response curve. We observed that the T_{heated} approach at 5 °C produces the highest signal gain with a $K_{1/2}$ of 12.8 ± 1.5 μM, which indicates that the thermal convection promotes aptamer binding to procaine at the temperature difference of 5 °C (Figure S4). Instead, the

https://doi.org/10.1021/acs.analchem.1c00289
Anal. Chem. 2021, 93, 7843−7850

Table 1. Dissociation Constant $K_{1/2}$ of Procaine-Binding E-AB Sensors at Different Temperatures

	$K_{1/2}$/μM	
T_s/°C	$T_{overall}$	T_{heated}
30	147.3 ± 14.2	259.5 ± 158.1
25	98.2 ± 5.6	134.3 ± 25.3
5	21.5 ± 2.4	12.8 ± 1.5
0	13.8 ± 1.5	

sensor becomes almost nonresponsive to procaine with the largest $K_{1/2}$ of 295.5 ± 158.1 μM at T_{heated} = 30 °C, showing that the thermal convection of 30 °C destabilizes the binding of the aptamer and target.

We demonstrated that the response of procaine sensors is a strong T_s-dependent function, producing "enhanced-responsive" and "~nonresponsive" signal outputs at given T_s = 5 and 30 °C, respectively (Figure 3A). The Au-TCDEs that are

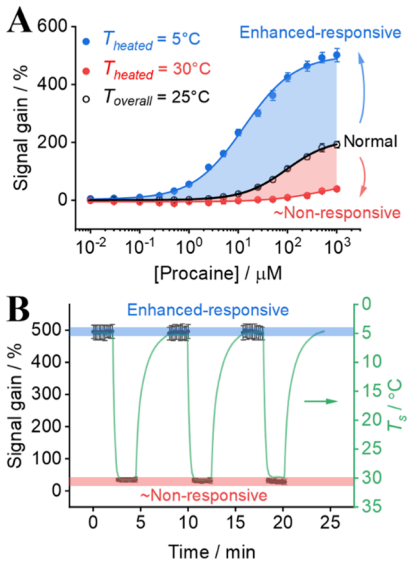

Figure 3. TAEAB sensors for the alternating cycle of "enhanced-responsive" or "~nonresponsive" state. (A) Compared with the performance at 25 °C, the signal of E-AB sensors can be greatly improved at T_{heated} = 5 °C (T_s = 5 °C, T_b = 0 °C), while it becomes almost nonresponsive to target molecules at T_{heated} = 30 °C (T_s = 30 °C, T_b = 0 °C). Here, the signal of 30 °C only changes a little at high target concentrations, so we described it as "~nonresponsive". (B) Response of procaine sensors changes alternately with the oscillation of T_s. The green line represents the T_s time curve. Here, T_s is converted by the open circuit potential method in 5 mM $K_3[Fe(CN)_6]/K_4[Fe(CN)_6]$ + 0.5 M KCl aqueous solution.[29] Au-TCDEs can rapidly, stably achieve the alternating temperature change of cold to hot on the electrode surface in an ice-water bath. The left axis represents the response of sensor changes at 5 or 30 °C with 500 μM procaine.

immersed in an ice-water bath can rapidly achieve the alternating temperature change of cold to hot on an electrode surface. For example, Au-TCDEs approximately need only 7 min to complete a 5−30−5 °C alternating temperature cycle (Figure 3B). Thus, we could control E-AB sensors from the state of the high sensitivity for target binding to the state of ~nonresponsive by adjusting T_s within a temporal resolution of a few minutes. To demonstrate this, the surface temperature of the aptamer-modified Au-TCDEs is oscillated between 5 and 30 °C, keeping 2 min for each temperature; then, the sensors record square wave signals in the presence of 500 μM procaine. As we predicted, the signal of E-AB sensors changes alternately with the oscillation of surface temperature (Figure 3B). Inspired by the dual frequency[4]/dual reporter[5,28] calibration-free sensing approach reported before, we described here a dual temperature alternating (DTA) strategy that exploits the voltammetric signal from a "~nonresponsive for target binding" temperature as a "reference" output, thus supporting calibration-free molecular measurements.

TA-EAB Sensor for Calibration-Free Molecular Measurements. To validate the DTA strategy here, we first applied it to a procaine-detecting TAEAB sensor in working buffer. We respectively collected SWV currents at 5 and 30 °C in the presence of different concentration targets, unsurprisingly observing a large variation in the peak currents for both i_5 and i_{30} (Figure S5A) with a reproducible ratio of these two (Figure S5B). Then, we fit the obtained response profiles with the Hill equation above to determine the "factory" parameters for a specific type of sensor[28] (*i.e.*, $K_{1/2}$, n, r_{min}, and r_{max}). Because of their good reproducibility, these parameters ($K_{1/2}$, n, r_{min}, and r_{max}) will be determined only one time and used for all these classes of sensors. The target concentration can be estimated from the measurements of α *via* a recast format of eq 1 below.

$$[\text{target}] = K_{1/2}\sqrt[n]{\frac{\alpha - r_{min}}{r_{max} - \alpha}} \quad (2)$$

where α is the ratio of i_5 and i_{30} (these two are the peak currents detected at 5 and 30 °C, respectively), r_{min} is the minimum value of α, and r_{max} is the maximum of α (*i.e.*, when the sensors are challenged in the absence or presence of a saturating target, respectively). We then applied these four parameters (Table S1) to a new set of procaine sensors, achieving procaine concentration estimates within 20% error over the range of 0.1 μM to 0.1 mM in buffer (Figure S5D). This is quite similar to the accuracy we achieve by calibrating the same sensors in a sample of known (here zero) target concentrations *via* the signal gain-corrected method (Figure S5D). We further challenged the other standard set of procaine sensors in undiluted urine. The peak currents or normalized signals (Figure S12A) observed for 5 and 30 °C vary dramatically across sensors, but their current ratio remains reproducible (Figures 4B, S12C). After defining $K_{1/2}$, n, r_{min}, and r_{max} for the sensors (Table S1), we recover procaine concentration estimates within 20% error over the range of 0.5 to 50 μM, achieving the accuracy of the traditional calibration approach (Figure 4C).

Cocaine[37] is one of the most abused drugs, and its concentration is approximately ~0.3 μM in urine when cocaine was administered after 60 h.[38] Procaine is used as a testing model to perform the calibration-free strategy due to the shortage of the high concentration cocaine samples (the related laws in China). To illustrate that our method is also applicable to cocaine detection, we compared the signal gain of these two target molecules under the best detection condition (Figure S6). Cocaine-detecting sensors have a better signal response at low concentrations. Our method could also support improved, sensitive, calibration-free cocaine measurements, at least achieving a detection limit of 0.5 μM in undiluted urine. Thus, we believe that our strategy can prolong

https://doi.org/10.1021/acs.analchem.1c00289
Anal. Chem. 2021, 93, 7843−7850

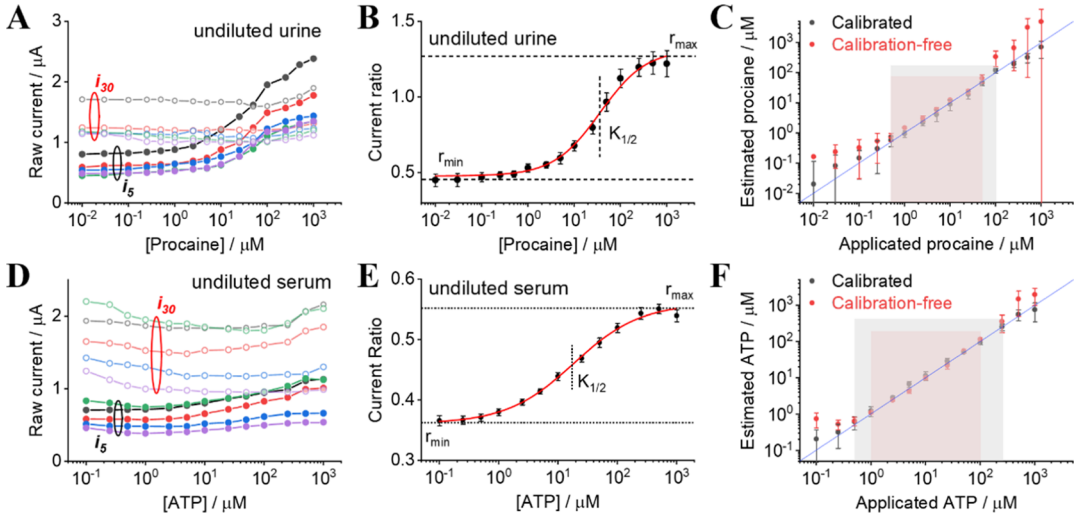

Figure 4. Temperature-alternated, small-molecule-detecting E-AB sensor for sensitive and calibration-free measurement in undiluted urine and serum. (A) We deployed a set of procaine-detecting sensors with their target in undiluted urine, observing significant variation in both i_5 and i_{30} (solid: i_5 hollow: i_{30}). (B) In contrast, the ratio α of the i_5 and i_{30} is quite reproducible from sensor to sensor. Using these data as our training set, we derived the parameters r_{min}, r_{max}, n, and $K_{1/2}$ for this class of sensors. (C) We then applied these parameters to a new set of sensors with a good recovery rate over 2 orders of magnitude concentration range (red symbols), a level of accuracy we achieved by calibrating the same sensors in a sample of zero target concentration (black symbols). (D) Challenging a training set of ATP-detecting, TAEAB sensors with their target in undiluted serum, we again observed significant variation in the absolute currents produced at 5 and 30 °C. (E) Ratio of their currents, however, is again quite reproducible from one sensor to the next. We then derived the parameters r_{min}, r_{max}, n, and $K_{1/2}$ from this set of titration data. (F) Applying these parameters to perform calibration-free measurements to a new, out-of-training-set group of sensors, we reproducibly achieved ATP concentration estimates within 16% error of the actual concentration across an approximate range from 1 to 100 μM, a level of accuracy similar to that achieved using the traditional calibration approach.

the effective detection time by improving the sensitivity of cocaine-detecting E-AB sensors.

As a validation of the generality of the DTA strategy reported here, we used it in E-AB sensors that recognize the ATP. Here, we have demonstrated that our strategy is also suitable to the ATP-detecting sensor (Figures S7−S11, Table S1). Similarly, because of the dependence of target-binding response on temperature (Figure S8), the relative response of the sensor is also a strong function of T_s, producing "enhanced-responsive" or "~nonresponsive" behaviors (Figure S10). First, we performed the calibration-free measurement in ATP working buffer (Figure S11). The ratio output estimated is accurate across an approximate 500-fold concentration range in working buffer (Figure S11C), a level of accuracy we achieved by calibrating the same sensors in a sample of zero target concentration. Similarly, we further challenged the other standard set of ATP sensors in undiluted serum (Figure S12B,D), with the estimated target concentrations across an approximately 100-fold concentration range of 1 to 100 μM (Figure 4D,F). The results mentioned above illustrate that TAEAB sensors can reproducibly estimate analyte concentration and significantly improve sensitivity without the need to calibrate each individual sensor.

Stability and Robustness of TAEAB Sensors. In addition to eliminating the need for end users to perform sensor calibration, the robustness and stability of ECBs are also essential for their practical application. We further challenged the stability and reusability of procaine and ATP TAEAB sensors for target measurement *in vitro*. We alternately detected two different procaine or ATP concentrations with every concentration for 60 min (measurement frequency of 6 min) over 10 h in undiluted urine or serum (Figure 5). A new set of TAEAB sensors accurately estimated the applied procaine or ATP concentration directly in the undiluted

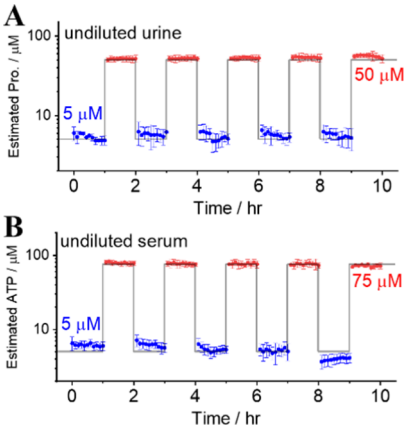

Figure 5. Stability of TAEAB sensors for the continuous multi-hour (A) procaine or (B) ATP molecule measurements *in vitro*. We interrogated the sensor for every 6 min over 10 h, with alternatively challenging it every 1 h with two different concentrations (gray trace: applicated concentration). The applicated target concentration can be directly estimated by eq 2 without the calibration operation (blue and red points: estimated concentration).

matrix without the calibrated operation, which shows the potential of our sensors in accurate, continuous target measurement.

Second, to test the long-term robustness of TAEAB sensors, the signal of ATP-detecting sensors was real-time monitored every 12 h over 2 weeks (Figure S13). We observed that ATP-detecting TAEAB sensors showed accurate and reproducible sensing behavior within 8 days after challenging with repeated measurement. Similarly, the target concentration estimations are in close agreement with the actual concentrations of the ATP spiked into the sample (Figure S13: black trace).

https://doi.org/10.1021/acs.analchem.1c00289
Anal. Chem. 2021, 93, 7843−7850

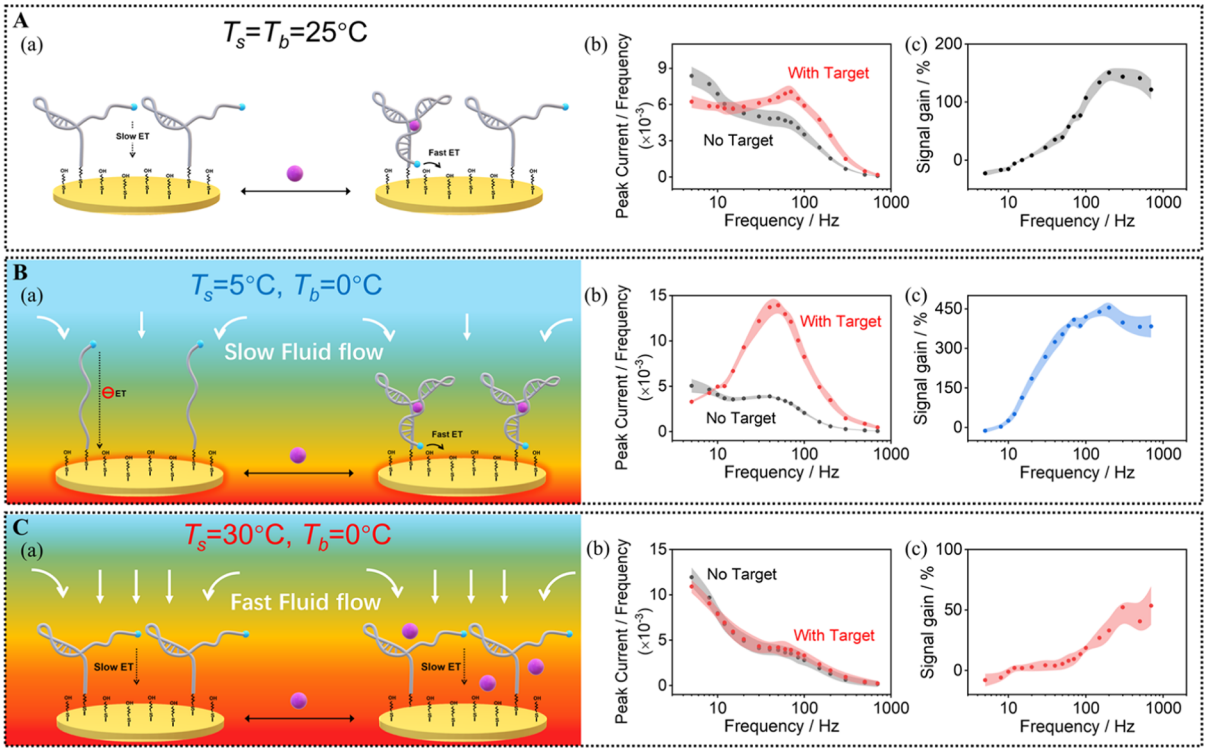

Figure 6. Mechanism of the DTA strategy. (A) $T_{overall}$ = 25 °C. (a) With 500 μM procaine (purple ball here), the target binding-induced conformational change alters the rate of ET from an attached redox reporter (MB, blue ball here). Obviously, compared with the variation of ET at 25 °C, the aptamer undergoes a greater change at (B) T_{heated} = 5 °C. Thermal convection in the condition of "5 °C" promotes the binding of the target and aptamer, resulting in the improving signal gain and sensitivity. However, at (C) T_{heated} = 30 °C, the convection will inhibit the binding of the target and aptamer. Here, the signal of 30 °C changes only a little at high target concentrations. The right panels (A–C, c) show the frequency-dependent signal gain upon the addition of 500 μM procaine. We use frequency 200 Hz to interrogate electrode and signal gain at different temperature conditions: (A) 151, (B) 465, and (C) 36%. The shaded areas indicate the error from at least three independently fabricated sensors.

Therefore, we demonstrated that TAEAB sensors have economic benefit due to the reusability and would be a promising testing platform for on-site biosensing and other applications.

Mechanism of the DTA Strategy. We discuss the mechanism of the DTA strategy in this section. As we described above, we believe that the primary reason for the T_s-dependent signal response is that the affinity of the aptamer is sensitive to temperature, especially for the structure-switching aptamer (it means the destabilization). Zou and Lou *et al.* reported that the cocaine aptamer at 25 °C has the higher affinity than that at 37 °C, and the triple-fragment cocaine aptamer will be binding to the target at 4 °C, but not binding at 25 °C.[34] Zhao *et al.* have demonstrated that the affinity of the different stem loop aflatoxin B1-binding aptamers can greatly improve at 4 °C.[36] Liu *et al.* also found that the binding of the dopamine aptamer became very tight at 5 °C.[39] Promoting the free aptamer of aqueous solution binding to the target can also translate to electrode surface behaviors at low temperatures. We then studied the relationship between the ET rate of MB and temperature for procaine-detecting sensors in working buffer. We estimated ET kinetics from the analysis of normalized peak currents extracted from voltammograms measured at different frequencies using the Lovrić approach[40,41] (Figure 6). The experimental results show the obvious change between the bound and unbound state of the ET (with or without 500 μM procaine) at both 25 and 5 °C, but a little change at 30 °C. If the ratio of the SWV peak current (I_p) and the frequency (f) depend parabolically on the log(f) with a maximum at a frequency, the ET rate can be calculated by the equation $k_s = \kappa_{max} f_{max}$ (Here, κ_{max} is a critical kinetic parameter that depends on the critical transfer coefficient and the square-wave amplitude).[42,43] Then, the ET of the bound state at 25 °C is estimated as 68.9 ± 6.7 s^{-1}, and the value of that at 5 °C is 44.2 ± 8.8 s^{-1} (nE_{SW} = 50 mV, k_{max} = 0.88, Figure S14). Although the ET rate of MB is reduced at low temperature, the response current dramatically increases with procaine at 5 °C (Figure S1A–C), suggesting that more aptamers undergo a conformational change.

This point was also proven by electrochemical impedance spectroscopy (EIS). EIS generally uses a free-solution redox reporter (typically $Fe(CN)_6^{3-/4-}$) that changes its charge transfer ability because of steric or electrostatic blocking of a functionalized electrode.[44] The related position change of the reporter will alter the charge transfer resistance (R_{ct}) of the free redox couple owing to the electrostatic attraction between the positively charged MB molecule and the negatively charged $Fe(CN)_6^{3-/4-}$probe.[45] We further characterized the effect of temperature on the self-assembly molecular layer by assessing R_{ct} of $Fe(CN)_6^{3-/4-}$ ions (Figure S15). We observed that R_{ct} of the redox couple greatly reduces when the target binds to the aptamer at 5 °C (Figure S15B). It indirectly indicates that the aptamer undergoes a more drastic conformational change or more aptamers bind to the target. However, the changes in R_{ct} were significantly weak with 500 μM procaine at 30 °C (Figure S15C).

Additionally, the interface temperature difference occurred between the electrode surface and bulk solution produces

https://doi.org/10.1021/acs.analchem.1c00289
Anal. Chem. 2021, 93, 7843–7850

completely different contributions for the signal of E-AB sensors at 5 or 30 °C (Figures S1 and S4). To illustrate it, COMSOL is used to simulate the heat and mass transfer around the electrode (Figure S16). According to the result of simulation, the aqueous solution flows upward from the bottom of the electrochemical cell to the electrode surface, resulting in an enhanced mass transport (thermal convection). The larger temperature difference will produce a faster flow rate of the convection. However, the thermal convection does reduce the response of the sensor at 30 °C. We believe that it is related to the binding affinity, namely, the interaction force of the aptamer and target at different temperatures. The binding force of the aptamer−target complex is tight due to the high affinity at 5 °C; thus, thermal convection promotes the binding of the target and aptamer and improves the signal response. The lower affinity will destabilize the bound state of the complex at 30 °C. Thus, the faster flow rate destabilizes the binding state of the aptamer and target, resulting in a nonresponse sensing behavior of E-AB sensors. To illustrate it, we explored the influence of rotating speed on the E-AB signal under the stirring state (the forced convection) at different temperatures in working buffer (Figure S17). The equilibrium state of the binding between the aptamer and target on the electrode surface is affected by the forced convection, resulting in the response variation of E-AB sensors. The same rotating speed (100 rpm) plays two roles for the response of sensors at 5 or 30 °C, which further demonstrated the abovementioned opinion.

CONCLUSIONS

To support POCT or on-site sensing, a sensor must achieve clinically acceptable accuracy and detection limit and yet simultaneously be convenient, rapid, and inexpensive.[46,47] Here, we demonstrate that temperature-alternated, E-AB sensors for the detection of small molecules can meet these demanding requirements. An inherent limitation to using the aptamer as a recognition element is that structure and function depend on environmental factors such as pH, temperature, and ionic strength.[48] Generally, it requires pretreatment samples (*e.g.*, using buffer to dilute) for maintaining the performance of the sensor.[24,27] Our strategy has achieved both signal enhancement and calibration-free measurement directly in unprocessed actual samples without needing reagent additions or other treatment steps. We only need to get the signal of the sensor at two different temperatures to directly estimate the target concentration. This method may be user-friendly and increase the convenience. With no sophisticated instrumentation, the temperature-alternating process utilizes the equipment readily available: inexpensive and easy-to-get ice-water bath, and commercially, the Au-TCDEs. Of note, the overall time of the detection process mainly comes from cooling of the sample solution (nearly 6 min). The measurement speed could be further increased by improving ice-water bath devices or using miniaturized electrodes. Given these arguments, we postulate that TAEAB sensors may significantly improve the clinical utility of many biosensors to extend their analytical applications in the areas of medical diagnostics, environmental monitoring, and food safety.

ASSOCIATED CONTENT

Supporting Information

The Supporting Information is available free of charge at https://pubs.acs.org/doi/10.1021/acs.analchem.1c00289.

Experimental procedures; electrode cleaning; sensor fabrication; temperature-dependent measurement of procaine and ATP E-AB sensors; calibration-free procaine and ATP in buffer; electrochemical impedance at different conditions and COMSOL simulation; and the influence of the rotating speed on the E-AB signal at different temperatures (PDF)

AUTHOR INFORMATION

Corresponding Authors

Jian-Jun Sun − *Ministry of Education Key Laboratory for Analytical Science of Food Safety and Biology, Fujian Provincial Key Laboratory of Analysis and Detection Technology for Food Safety, College of Chemistry, Fuzhou University, Fuzhou, Fujian 350108, China;* orcid.org/0000-0002-7987-5242; Phone: +86 591 22866136; Email: jjsun@fzu.edu.cn

Sen Yang − *Ministry of Education Key Laboratory for Analytical Science of Food Safety and Biology, Fujian Provincial Key Laboratory of Analysis and Detection Technology for Food Safety, College of Chemistry, Fuzhou University, Fuzhou, Fujian 350108, China; Key Laboratory of Targeting Therapy and Diagnosis for Critical Diseases Collaborative Innovation Center of New Drug Research and Safety Evaluation, School of Pharmaceutical Sciences, Zhengzhou University, Zhengzhou 450001, China;* Email: senyang@zzu.edu.cn

Authors

Zhi-min Chen − *Ministry of Education Key Laboratory for Analytical Science of Food Safety and Biology, Fujian Provincial Key Laboratory of Analysis and Detection Technology for Food Safety, College of Chemistry, Fuzhou University, Fuzhou, Fujian 350108, China*

Yi Wang − *Ministry of Education Key Laboratory for Analytical Science of Food Safety and Biology, Fujian Provincial Key Laboratory of Analysis and Detection Technology for Food Safety, College of Chemistry, Fuzhou University, Fuzhou, Fujian 350108, China*

Xing-yuan Du − *Ministry of Education Key Laboratory for Analytical Science of Food Safety and Biology, Fujian Provincial Key Laboratory of Analysis and Detection Technology for Food Safety, College of Chemistry, Fuzhou University, Fuzhou, Fujian 350108, China*

Complete contact information is available at: https://pubs.acs.org/10.1021/acs.analchem.1c00289

Notes

The authors declare no competing financial interest.

ACKNOWLEDGMENTS

The authors are thankful for the financial support from the National Science Foundation of China (grant no. 21874021), the Natural Science Foundation of Fujian Province, China (grant no. 2019J01205), and the Open Project Program of the State Key Laboratory of Photocatalysis on Energy and Environment (grant no. SKLPEE-202020). We also gratefully acknowledge the valuable advice about E-AB sensors from Prof. Yi Xiao (Florida International University).

https://doi.org/10.1021/acs.analchem.1c00289
Anal. Chem. 2021, 93, 7843−7850

REFERENCES

(1) Schneider, F.; Maurer, C.; Friedberg, R. C. *Ann. Lab. Med.* **2017**, *37*, 365−370.
(2) Acciaroli, G.; Vettoretti, M.; Facchinetti, A.; Sparacino, G. *Diabetes Technol. Ther.* **2018**, *20*, 59−67.
(3) Kim, J.; Kim, M.; Lee, M.-S.; Kim, K.; Ji, S.; Kim, Y.-T.; Park, J.; Na, K.; Bae, K.-H.; Kim, H. K. *Nat. Commun.* **2017**, *8*, 14997.
(4) Li, H.; Dauphin-Ducharme, P.; Ortega, G.; Plaxco, K. W. *J. Am. Chem. Soc.* **2017**, *139*, 11207−11213.
(5) Li, H.; Li, S.; Dai, J.; Li, C.; Zhu, M.; Li, H.; Lou, X.; Xia, F.; Plaxco, K. W. *Chem. Sci.* **2019**, *10*, 10843−10848.
(6) Song, S.; Wang, L.; Li, J.; Fan, C.; Zhao, J. *TrAC, Trends Anal. Chem.* **2008**, *27*, 108−117.
(7) Campuzano, S.; Yáñez-Sedeño, P.; Pingarrón, J. M. *Curr. Opin. Electrochem.* **2019**, *16*, 35−41.
(8) Hoekstra, R.; Blondeau, P.; Andrade, F. J. *Anal. Bioanal. Chem.* **2018**, *410*, 4077−4089.
(9) Bakker, E. *ACS Sens.* **2016**, *1*, 838−841.
(10) Campuzano, S.; Pedrero, M.; Gamella, M.; Serafín, V.; Yáñez-Sedeño, P.; Pingarrón, J. M. *Sensors* **2020**, *20*, 3376.
(11) Gooding, J. J. *ACS Sens.* **2018**, *3*, 1609.
(12) Bakker, E. *ACS Sens.* **2018**, *3*, 1431.
(13) Mayer, M.; Baeumner, A. J. *Chem. Rev.* **2019**, *119*, 7996−8027.
(14) Gutiérrez-Sanz, Ó.; Haustein, N.; Schroeter, M.; Oelschlaegel, T.; Filipiak, M. S.; Tarasov, A. *Sens. Actuators, B* **2019**, *295*, 153−158.
(15) Xiao, Y.; Lubin, A. A.; Heeger, A. J.; Plaxco, K. W. *Angew. Chem.* **2005**, *117*, 5592−5595.
(16) Hui, L.; Jacob, S.; Fan, X.; Plaxco, K. W. *Anal. Chem.* **2018**, *90*, 10641.
(17) Liang, S.; Kinghorn, A. B.; Voliotis, M.; Prague, J. K.; Veldhuis, J. D.; Tsaneva-Atanasova, K.; McArdle, C. A.; Li, R. H. W.; Cass, A. E. G.; Dhillo, W. S.; Tanner, J. A. *Nat. Commun.* **2019**, *10*, 852.
(18) Dauphin-Ducharme, P.; Yang, K.; Arroyo-Currás, N.; Ploense, K. L.; Zhang, Y.; Gerson, J.; Kurnik, M.; Kippin, T. E.; Stojanovic, M. N.; Plaxco, K. W. *ACS Sens.* **2019**, *4*, 2832−2837.
(19) Fan, C.; Plaxco, K. W.; Heeger, A. J. *Proc. Natl. Acad. Sci. U.S.A.* **2003**, *100*, 9134−9137.
(20) Arroyo-Currás, N.; Somerson, J.; Vieira, P. A.; Ploense, K. L.; Kippin, T. E.; Plaxco, K. W. *Proc. Natl. Acad. Sci. U.S.A.* **2017**, *114*, 645.
(21) White, R. J.; Plaxco, K. W. *Anal. Chem.* **2010**, *82*, 73−76.
(22) Lubin, A. A.; Plaxco, K. W. *Acc. Chem. Res.* **2010**, *43*, 496−505.
(23) Ricci, F.; Vallée-Bélisle, A.; Simon, A. J.; Porchetta, A.; Plaxco, K. W. *Acc. Chem. Res.* **2016**, *49*, 1884−1892.
(24) Yu, H.; Chen, Z.; Liu, Y.; Alkhamis, O.; Song, Z.; Xiao, Y. *Angew. Chem.* **2021**, *133*, 3030.
(25) Dauphin-Ducharme, P.; Plaxco, K. W. *Anal. Chem.* **2016**, *88*, 11654−11662.
(26) Dauphin-Ducharme, P.; Yang, K.; Arroyo-Currás, N.; Ploense, K. L.; Zhang, Y.; Gerson, J.; Kurnik, M.; Kippin, T. E.; Stojanovic, M. N.; Plaxco, K. W. *ACS Sens.* **2019**, *4*, 2832−2837.
(27) Idili, A.; Parolo, C.; Ortega, G.; Plaxco, K. W. *ACS Sens.* **2019**, *4*, 3227−3233.
(28) Zhu, M.; Li, S.; Li, H.; Li, H.; Xia, F. *Anal. Chem.* **2020**, *92*, 12437−12441.
(29) Yang, S.; Chen, X.; Mi, Z.-Z.; Chen, Z.-M.; Li, X.-D.; Sun, J.-J.; Wu, S.-H. *ACS Sens.* **2019**, *4*, 1594−1602.
(30) Marken, F.; Tsai, Y.-C.; Coles, B. A.; Matthews, S. L.; Compton, R. G. *New J. Chem.* **2000**, *24*, 653−658.
(31) Beckmann, A.; Coles, B. A.; Compton, R. G.; Gründler, P.; Marken, F.; Neudeck, A. *J. Phys. Chem. B* **2000**, *104*, 764−769.
(32) Wang, Z.; Yu, H.; Canoura, J.; Liu, Y.; Alkhamis, O.; Fu, F.; Xiao, Y. *Nucleic Acids Res.* **2018**, *46*, No. e81.
(33) White, R. J.; Rowe, A. A.; Plaxco, K. W. *Analyst* **2010**, *135*, 589−594.
(34) Zou, R.; Lou, X.; Ou, H.; Zhang, Y.; Wang, W.; Yuan, M.; Guan, M.; Luo, Z.; Liu, Y. *RSC Adv.* **2012**, *2*, 4636−4638.
(35) Amano, R.; Takada, K.; Tanaka, Y.; Nakamura, Y.; Kawai, G.; Kozu, T.; Sakamoto, T. *Biochemistry* **2016**, *55*, 6221−6229.
(36) Wang, C.; Liu, L.; Zhao, Q. *ACS Sens.* **2020**, *5*, 3246−3253.
(37) Schramm, W.; Craig, P. A.; Smith, R. H.; Berger, G. E. *Clin. Chem.* **1993**, *39*, 481−487.
(38) Jufer, R. A.; Wstadik, A.; Walsh, S. L.; Levine, B. S.; Cone, E. J. *J. Anal. Toxicol.* **2000**, *24*, 467−477.
(39) Liu, X.; Hou, Y.; Chen, S.; Liu, J. *Biosens. Bioelectron.* **2021**, *173*, 112798.
(40) Curtis, S. D.; Ploense, K. L.; Kurnik, M.; Ortega, G.; Parolo, C.; Kippin, T. E.; Plaxco, K. W.; Arroyo-Currás, N. *Anal. Chem.* **2019**, *91*, 12321−12328.
(41) Mirčeski, V.; Lovrić, M. *Electroanalysis* **1997**, *9*, 1283−1287.
(42) Komorsky-Lovrić, Š.; Lovrić, M. *Anal. Chim. Acta* **1995**, *305*, 248−255.
(43) Abi, A.; Ferapontova, E. E. *J. Am. Chem. Soc.* **2012**, *134*, 14499−14507.
(44) Daniels, J. S.; Pourmand, N. *Electroanalysis* **2007**, *19*, 1239−1257.
(45) Xiao, Q.; Li, J.; Jin, X.; Liu, Y.; Huang, S. *Sens. Actuators, B* **2019**, *297*, 126740.
(46) Vashist, S. K.; Luppa, P. B.; Yeo, L. Y.; Ozcan, A.; Luong, J. H. T. *Trends Biotechnol.* **2015**, *33*, 692−705.
(47) Luppa, P. B.; Müller, C.; Schlichtiger, A.; Schlebusch, H. *TrAC, Trends Anal. Chem.* **2011**, *30*, 887−898.
(48) Schoukroun-Barnes, L. R.; Macazo, F. C.; Gutierrez, B.; Lottermoser, J.; Liu, J.; White, R. J. *Annu. Rev. Anal. Chem.* **2016**, *9*, 163−181.

https://doi.org/10.1021/acs.analchem.1c00289
Anal. Chem. 2021, 93, 7843−7850